September 2026
Volume 2
Issue 4

DOI: 10.48308/ijce.2026.247778.1038

Member Design Utilization for BIM Clash Review Prioritization: A Graph-Based Framework with Non-Compensatory Review Constraints

Authors:

Mehdi Shahraki[1,*], Roozbeh Hamidi[1]

Abstract

Geometric overlap identifies candidate clashes but gives engineers little information about the utilization of the affected member. We examined how linking design records to clash pairs changes the composition of a fixed review queue. For one building in Mashhad, Iran, we aggregated 11,438 Navisworks occurrences into 7,296 filtered pairs and linked Revit elements to ETABS members. Direct and segment-based matches covered 377 of 4,832 structural pairs (7.80%) across 120 beams. None of the 17 composite beams with strength ratios at or above unity had an accepted beam match. At a budget of 38 pairs, introducing member utilization increased median utilization from 0.3850 under controlled ablation to 0.7885 and reduced beam coverage from 23 to 19. The resulting queue shared 18 pairs with the ablation queue and 16 with the geometry–network queue. In a conditional extension, a mandatory review rule selected nine pairs associated with one candidate built-up column. These results quantify changes in review workload within the mapped subset. Independent engineering urgency ratings and physical connection details remain outstanding.

Keywords: Building Information Modeling, Clash Prioritization, Member Design Utilization, Graph Analysis, Engineering Review

1. Department of Civil Engineering, Islamic Azad University, Zahedan Branch, Zahedan, Iran

*Corresponding Author: Mehdi.shahraki@iau.ac.ir

Copyright: © 2026 by the authors. Submitted for possible open access publication under the terms and conditions of the Creative Commons Attribution (CC BY 4.0) International License (https://creativecommons.org/licenses/by/4.0/).

1. Introduction

Federated building information models enable designers to identify conflicts before construction. A clash report, however, does not establish which member should be reviewed first. A single member may generate numerous records, and a shallow intersection may involve a primary load-bearing element. The benefits and implementation of BIM are discussed by Bryde et al. (2013), Succar (2009), and Sacks et al. (2018). Akponeware and Adamu (2017) and Pärn et al. (2018) examine the coordination problems underlying clashes. Identifying a conflict and approving a structural modification remain separate engineering tasks.

Penetration depth measures geometric overlap. A strength utilization ratio, in contrast, expresses the demand relative to a particular design resistance or interaction limit. An overlap with a modeled room volume may have no physical consequence, whereas even a shallow clash involving a heavily utilized member warrants scrutiny. Neither measure alone determines the residual resistance of a member after modification.

Previous work has addressed component networks, multi-criteria prioritization, and machine learning for clash management (Hu et al., 2019, 2020, 2021; Bitaraf et al., 2024; Ailem & Boton, 2026; Koo et al., 2026; Yu et al., 2026). Abbasnejad et al. (2026) discuss the need for accountable decision support and further validation. An unresolved engineering question is how to use analytical design results without assigning them to the wrong physical member.

This study examines how the ranking of BIM clash pairs changes when geometric and network descriptors are supplemented by member-level design utilization. A further question is whether a weighted score can conceal cases that warrant structural review. To address this problem, a separate rule flags mapped ratios at or above unity, regardless of the geometric score.

The main contribution is the combination of traceable physical-to-analytical mapping and a non-compensatory review rule. Direct and segment-based correspondence are distinguished from conditional built-up column mapping. Ranking changes are evaluated at a fixed review budget, while an additive score provides the contribution of each criterion. Unsupervised clustering is used to examine the structure of the dataset rather than to assign risk labels. Sections 2–5 describe the literature, case study, mapping, and decision model. Section 6 presents the results; Section 7 summarizes the findings.

2. Literature Review and Research Gap

2.1. From Geometric Detection to Reviewable Issues

Information management and exchange standards support coordination of federated models (International Organization for Standardization, 2018, 2024). They do not equate clash penetration with a structural limit state. Mehrbod et al. (2019) examine the representation and

resolution of coordination issues beyond isolated clashes. A unique element pair is a useful unit of analysis, provided that the original occurrences remain accessible for local review.

Lin and Huang (2019) combine rules with machine learning to filter irrelevant clashes. Ailem and Boton (2026) investigate machine-learning relevance filtering, whereas Yu et al. (2026) examine penetration and constructability classification using multi-view transformer learning. The present study first excludes room-volume pairs using semantic information. Retention in the dataset does not, by itself, establish that a pair needs physical correction.

2.2. Network Representation and Resolution Dependencies

In a clash graph, vertices represent elements and edges represent encounters. Degree describes the number of distinct neighboring elements; betweenness reflects the position of a vertex on network paths (Freeman, 1979; Newman, 2010). These measures can reveal coordination concentrations but do not describe structural load transfer.

Hu et al. (2019, 2020, 2021) examine component networks, correction sequences, and change prediction. Hu et al. (2023) use graph convolution for change prediction in MEP models, while Liu et al. (2024) investigate multi-objective clash resolution using NSGA-II. These approaches address which objects to change or how to organize corrections. The present work addresses an earlier decision: which encounters should be reviewed by an engineer.

Harode et al. (2024) investigate prediction of clash-resolution options. Teo et al. (2022) examine BIM-enabled MEP coordination and management strategies. A review queue can support these processes, but an observed shared-element relation cannot establish the consequences of an untested correction.

2.3. Multi-Criteria Assessment and Structural Information

Hasannejad et al. (2022) investigate fuzzy-AHP for relevance prioritization. Bitaraf et al. (2024) and Bitaraf and Shirzadi Javid (2024) apply the best–worst method (BWM; Rezaei, 2015). Expert-derived importance ratings reflect coordination preferences, but two members of the same category can have very different design ratios. Conversely, a member ratio does not measure the difficulty of resolving an interference.

A weighted sum allows a low value of one criterion to offset a high value of another. Such trade-offs are useful for general coordination but can be inappropriate when an analytical design check requires attention. A reported ratio at or above unity is therefore treated here as a separate review trigger. Its interpretation still depends on the check type, model identity, and design settings.

2.4. Unsupervised Analysis and Transparent Decisions

Gower (1971) defines a distance suitable for mixed attributes. Hierarchical and density-based methods can then identify groups without predefined labels (Campello et al., 2013; McInnes et al., 2017). The silhouette coefficient measures separation in the selected feature space (Rousseeuw, 1987). Including member category may, however, produce clusters that simply reproduce the existing classification.

Borkowski and Kubrat (2026) propose a conceptual AI-based triage framework, and Koo et al. (2026) examine clash relevance and risk using machine learning. For decisions that require engineering accountability, a transparent model is preferable when its assumptions can be stated directly (Rudin, 2019). The present score requires neither training labels nor a neural network.

Table 1 compares the decision targets of the selected studies. It provides a methodological comparison rather than a quantitative benchmark, since the methods were not evaluated on identical data.

Table 1. Comparison of selected BIM clash management approaches

Study	Primary method or task	Distinction from this study
Hu et al. (2019, 2020)	Component networks; correction sequencing	Review priority, not causal correction order
Hu et al. (2021, 2023)	Graph-based change prediction; GCN	Direct score, no learned change prediction
Hasannejad et al. (2022)	Fuzzy-AHP relevance prioritization	Mapped analytical design evidence
Bitaraf et al. (2024)	Expert BWM and contextual factors	Member-level ratios; explicit escalation
Liu et al. (2024)	Multi-objective resolution	No proposed geometric correction
Ailem & Boton (2026); Yu et al. (2026)	ML-based filtering/classification	Ordering review after semantic screening
Koo et al. (2026)	Risk and relevance analysis	No supervised risk prediction
Borkowski & Kubrat (2026)	Conceptual AI triage	Single-case computational implementation
Present study	Graph, utilization and review constraint	Confidence-aware mapping and auditable queue

Published workflows already prioritize and group clashes. The question addressed here is narrower: how do correspondence confidence, member-level utilization, and an obligatory referral threshold change which cases enter a fixed review budget?

The research gap concerns the use of member-level design results under incomplete model correspondence. In particular, geometric and network criteria may offset a high mechanical value in a compensatory score. The proposed method addresses both issues by retaining mapping confidence and separating mandatory review from the weighted ranking.

3. Case Study and BIM Data Acquisition

3.1. Study Design and Building Models

The case study is a residential building in Honarestan, Mashhad, Iran. The physical BIM comprises architectural, structural, and mechanical, electrical, and plumbing (MEP) models. The analytical frame contains composite and non-composite beams, steel columns, and braces. Existing models of the same building provided the geometric basis; the contribution of this study lies in the subsequent mapping and review analysis.

Figure 1 outlines the procedure. The clash records are first aggregated and screened, after which a graph is constructed. ETABS design ratios enter a separate correspondence procedure. Mechanical ranking is restricted to pairs with accepted or explicitly conditional matches. The clustering branch describes the resulting feature patterns and does not feed cluster labels into the score.

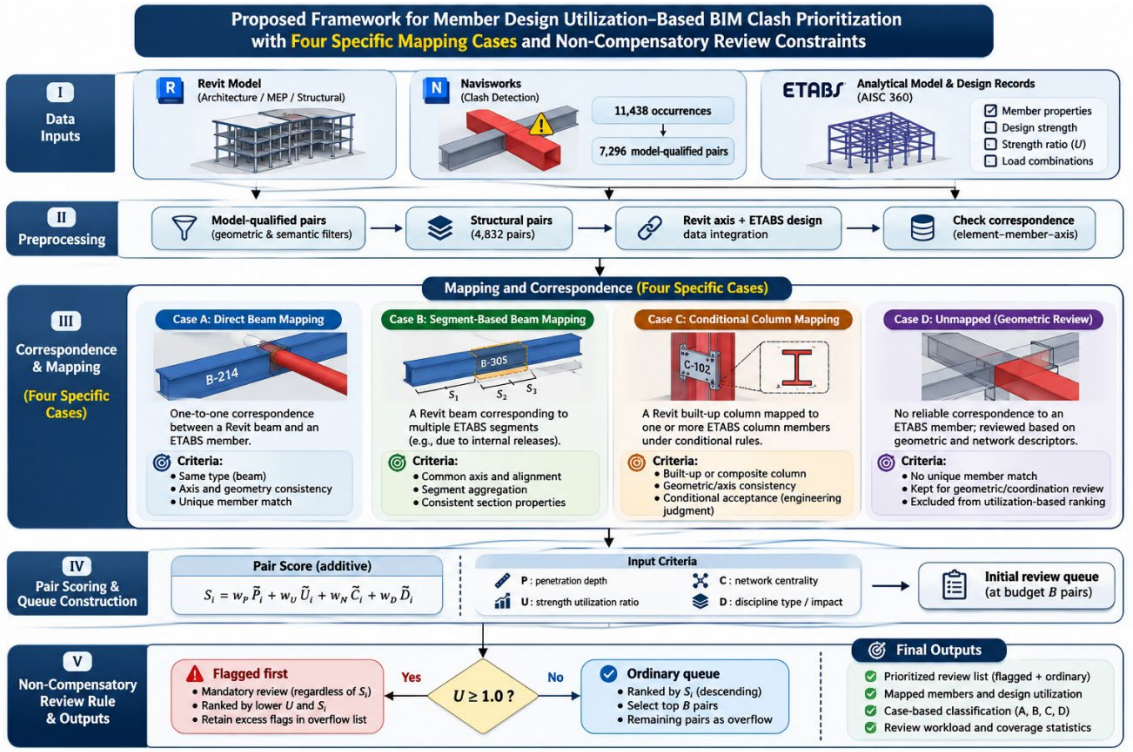

Figure 1. Workflow for traceable design-informed structural clash review.

Figure 2 shows the Revit structural model and first-floor plan. The vertical arrangement of the framing and the grid intersections provide geometric references for matching physical and analytical members. The images alone cannot establish seismic adequacy or the classification of the lateral-force-resisting system.

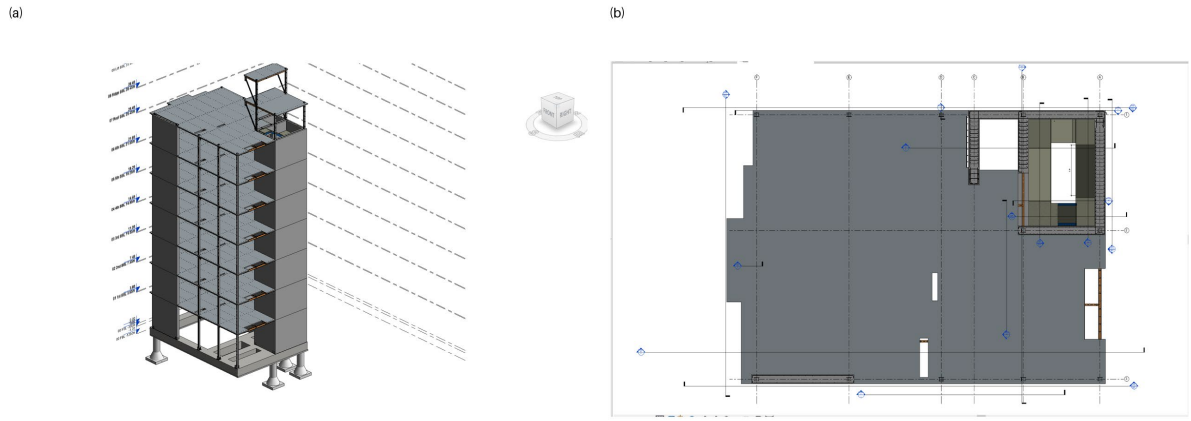

Figure 2. Physical structural model in Revit: (a) three-dimensional view; (b) first-floor plan and grid.

3.2. Analytical Design Records

The final analytical model contains 1,190 joints and 413 distinct frame members. These comprise 294 composite beams, 28 non-composite beams, 84 steel columns, and seven braces. The design export contains 427 records before aggregation by member identifier. Table 2 summarizes the recorded strength ratios. The steel and composite beam design records specify AISC 360-05 and AISC 360-10, respectively (American Institute of Steel Construction, 2005, 2010). These are the recorded design editions, not evidence of compliance with current provisions.

Table 2. Analytical frame member inventory and recorded strength utilization

Member family	Count	Minimum	Median	Maximum	U ≥ 1
Composite beam	294	0.007	0.3850	1.937	17
Steel beam	28	0.110	0.2965	0.749	0
Steel column	84	0.055	0.5455	1.001	1
Brace	7	0.021	0.0220	0.040	0
Total	413	—	—	—	18

All 413 frame identifiers and their end-joint connections agree between the earlier and final analytical definitions. The largest joint-coordinate change is 16.844 mm. However, 20 beams changed section from IPE140, IPE160, or IPE180 to IPE300. These changes were not accepted

for mapping without confirmation of the physical counterpart. Consequently, an unchanged identifier does not establish that a recorded design ratio belongs to the section visible in the clash model.

3.3. Clash Observations and Semantic Filtering

Hard-clash reports were obtained for structure–MEP, architecture–MEP, and structure–architecture tests at a recorded tolerance of zero. Each occurrence identifies two elements, a representative location, and a signed distance. Reported status labels were preserved as workflow attributes. Figure 3 shows the federated model and a local clash. The colored highlights identify the involved objects but do not establish material loss or local stresses.

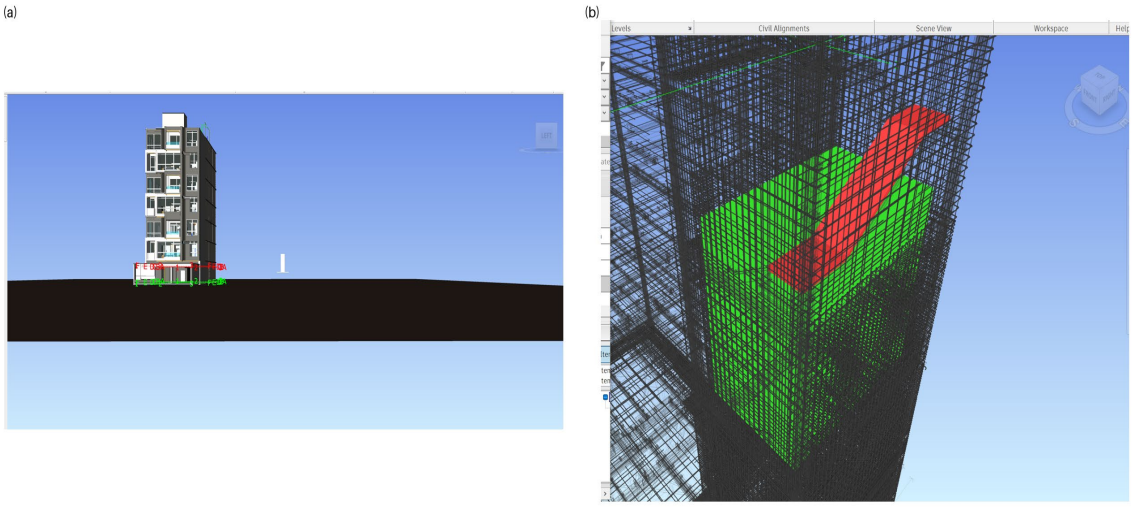

Figure 3. Navisworks records: (a) federated building view; (b) example of a local geometric interference.

Identical numerical identifiers can occur in different discipline models. To avoid conflating distinct elements, Eq. (1) combines the source model, model(e), with the element identifier, id(e).

$$K_e = \left(\text{model}(e), \text{id}(e)\right) \tag{1}$$

The test identifier and the unordered pair of element keys define the analysis record. All underlying occurrences are preserved for later location checks. For pair c, with occurrence set R(c), Eq. (2) gives the maximum absolute recorded distance in millimeters.

$$d(c) = 1000 \max_{j \in R(c)} |s_j| \tag{2}$$

Here, s_j is the signed distance of occurrence j in meters. All available hard-clash distances are nonpositive, including zero. Maximum penetration provides a consistent geometric descriptor,

not the volume of material to be removed. Preserving the occurrence locations is especially important when one physical element spans several analytical segments.

Table 3 reconciles occurrence counts, unique pairs, and semantic exclusions. Pairs involving room volumes were excluded based on their element category, not their penetration depth or status.

Table 3. Reconciliation of raw occurrences, unique pairs and semantic filtering

Discipline pair	Raw	Unique	Filtered	Filtered share (%)
Structure–MEP	296	287	287	3.93
Architecture–MEP	3978	2978	2464	33.77
Structure–architecture	7164	4808	4545	62.29
Total	11438	8073	7296	100.00

After filtering, 7,296 pairs remain, corresponding to 10,352 retained occurrences. Of these pairs, 612 have multiple occurrences. The 4,832 pairs involving structural elements form the population for structural screening. Aggregation and semantic exclusion account for the reduction in counts; no physical clash correction is implied.

4. Physical-to-Analytical Structural Model Mapping

4.1. Information Provenance and Coordinate Transformation

Assigning a design ratio requires correspondence between the physical element in the clash record and an analytical member. Navisworks provides the element pair, occurrence history, position, and distance. Revit provides physical identifiers, categories, axes, section descriptions, and bounding information. ETABS supplies connectivity, analytical axes, section labels, and design results. The dataset contains 7,088 extracted Revit elements. All 1,184 distinct structural elements in the clash reports were located in that inventory, but this confirms only physical-model lookup.

The proposed transformation comprises a 90° horizontal rotation and a translation. It assumes consistent Navisworks and Revit reporting frames. Equation (3) expresses the transformed coordinates in meters.

$$X_E = -Y_R, \quad Y_E = X_R + 14.535, \quad Z_E = Z_R + 0.30 \tag{3}$$

Three grid intersections used to establish the transform have residual magnitudes of 65 mm each. Eight additional Story2 intersections were checked against identified ETABS joint

coordinates using the 7.40 m Revit BSL and the 7.70 m analytical level (Supplementary Table S1). With the fitted transform held fixed, vector RMSE was 49.50 mm, and the largest residual was 95.52 mm at A-2. Both 70 mm transverse residuals occur on grid 2. Across 104 candidate joint–grid matches from base to roof, RMSE was 77.82 mm, and the maximum was 215 mm on Revit grid C. Repeated levels reuse the same plan grid. These tests quantify internal alignment under the proposed grid identities; independently identified physical control points are still needed.

Figure 4 presents ETABS design views for steel and composite members. The numerical design records, rather than contour colors, supply the mechanical values for ranking.

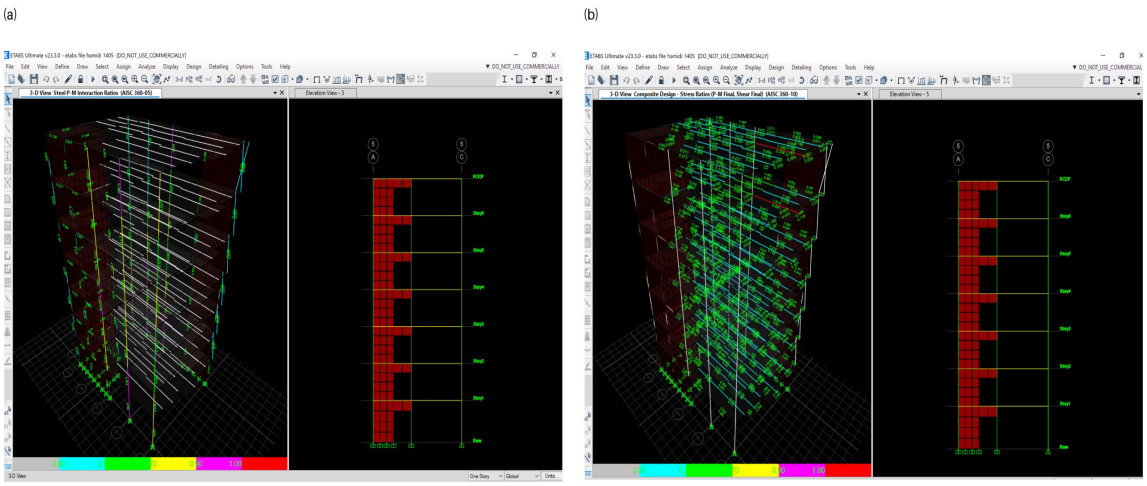

Figure 4. Analytical model design output: (a) steel interaction ratios; (b) composite beam strength checks.

4.2. Direct Correspondence

Let s and t be the transformed physical endpoints and a and b the analytical endpoints. Their order may differ between software models. Equation (4) therefore evaluates both orientations and retains the smaller maximum endpoint discrepancy.

$$e = \min\{\max(\| a - s \|, \| b - t \|), \max(\| a - t \|, \| b - s \|)\} \quad (4)$$

Direct mapping requires an absolute direction cosine greater than 0.995 and an endpoint error no greater than 0.15 m. The next-best candidate must have an error at least 0.10 m larger. Normalized section descriptions must agree, and unresolved section changes are excluded. These thresholds are mapping parameters, not construction tolerances.

Scenario A links 109 physical elements to 109 analytical members and covers 329 clash pairs. The correspondence remains dependent on the adopted coordinate transformation.

4.3. Segment-Based Beam Correspondence

Physical and analytical models may subdivide the same beam differently. Let L be the analytical length and l and h the lower and upper projections of the transformed physical endpoints along its axis. Equation (5) gives the overlap length and its normalized value; L_R denotes the physical-axis length.

$$l_o = \max\big(0, \min(L, h) - \max(0, l)\big), \quad \eta = \frac{l_o}{\min(L, L_R)} \tag{5}$$

Segment mapping requires an axis separation of at most 0.15 m, an overlap ratio of at least 0.90, and compatible directions and sections. All occurrence points must lie within the common interval, allowing a 0.10 m end margin. Candidates within 0.05 m of the best axis distance were rejected as ambiguous. This step adds 48 pairs from 18 physical elements and 11 analytical beams. Scenario B consequently includes 377 pairs and 120 analytical members.

4.4. Built-Up Column Correspondence

A built-up column may be represented by several physical profiles but by one analytical section. The interaction ratio of the assembly cannot be assigned to an individual profile as its own resistance check. Candidate IPE14 axes were searched within 0.20 m of the analytical axis at the clash locations and the segment midpoint. Additional requirements were a centroid offset of at most 0.10 m, profile separation of at least 0.035 m, a distance greater than 0.05 m from segment boundaries, and assembly membership.

Of 284 elevation-based candidates, 145 passed the assembly screen. They involve 20 physical elements and 28 analytical segments. These matches define scenario C, which remains conditional because complete section properties and connections were not independently verified.

Figure 5 shows the exported footprints of the three Revit profiles and the two axes. Their story-level correspondence was checked against the analytical connectivity.

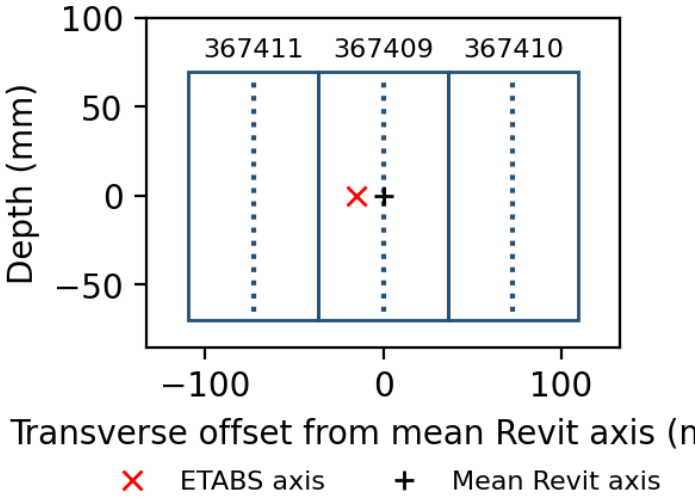

Figure 5. Exported profile bounding boxes and axis positions at D-3. Outlines show bounding extents; internal steel geometry and connectors are unspecified.

For Story2/C12, ETABS connects joints 29 and 677 along (10.450, 7.750) m from elevation 4.10 to 7.70 m. Three Revit IPE140 profiles (367409–367411) have transformed centerlines 73 mm apart, with a mean axis at (10.450, 7.765) m. The measured plan offset is 15 mm. The profiles span 219 mm overall and are 140 mm deep. The ST37 analytical general section has the same width, a depth of 156 mm, and an assigned area of 7,800 mm². The 16 mm depth difference does not establish the presence or thickness of plates. Capacity of the physical assembly and force transfer between profiles remain unverified.

4.5. Member Design Utilization and Missing Values

The mechanical variable is the maximum valid reported strength ratio of the corresponding member. Member family and check type are retained alongside the ratio. Equation (6) defines the steel-member indicator.

$$U_s = \max\left(r_{PMM}, r_{V,major}, r_{V,minor}\right) \tag{6}$$

The terms in Eq. (6) are the axial–flexural interaction and major- and minor-axis shear ratios. Equation (7) defines the composite-beam indicator from construction-stage, final-stage, and stud checks.

$$U_c = \max\left(r_{Str,PM}, r_{Str,V}, r_{Const,PM}, r_{Const,V}, r_{Stud}\right) \tag{7}$$

Str and Const refer to final strength and construction stages, respectively. Serviceability checks are considered separately. Missing or invalid ratios are not assigned zero. U(c) is a member-level design indicator rather than a local residual strength.

Table 4 defines the nested mechanical populations. Scenario B provides the principal beam-based comparison; scenario C extends it to conditional column matches and is used to examine the mandatory review rule.

Table 4. Nested mapping scenarios and evidence levels

Scenario	Pairs	Unique members	Coverage (%)	Interpretation
A – direct	329	109	6.81	Endpoint and section rules
B – beams	377	120	7.80	A + segment mapping
C – extended	522	148	10.80	B + conditional columns
Not mapped in C	4310	—	89.20	No assigned utilization

Coverage is measured against the 4,832 structural pairs. Even in C, 4,310 pairs lack a mechanical match. These cases retain a separate geometric–network screening route rather than being treated as structurally unimportant.

5. Graph-Based Structural Review Prioritization Framework

5.1. Graph Definition and Features

The retained element pairs form an undirected simple graph G = (V, E). Vertices are composite physical identifiers; edges are distinct pairs. Repeated occurrences remain attached to each edge. Equation (8) defines the symmetric adjacency matrix A and degree k_i of vertex i.

$$A_{ij} = \begin{cases} 1 & \{i,j\} \in E \\ 0 & \text{otherwise} \end{cases}, \quad k_i = \sum_j A_{ij} \tag{8}$$

For an edge c between vertices i and j, N(c) counts the other edges sharing either endpoint. Equation (9) defines this feature and the normalized vertex degree C_D.

$$C_D(i) = \frac{k_i}{|V|-1}, \quad N(c) = k_i + k_j - 2 \tag{9}$$

Betweenness was approximated using 128 sources and seed 2026. The line graph contains $\Sigma\, k_i(k_i-1)/2$ shared-element adjacencies. Each represents a possible coordination relationship, not a demonstrated dependency between corrections.

5.2. Unsupervised Characterization

Mixed attributes were compared using Gower distance. Numerical differences are scaled by feature range; categorical differences are represented by zero or one. Equation (10) expresses the weighted distance over the features available for a pairwise comparison.

$$D_{ij} = \frac{\sum_k w_k \delta_{ijk}}{\sum_k w_k} \tag{10}$$

Average-linkage clustering was evaluated using silhouette. A numerical-only variant with equal feature weights and HDBSCAN sensitivity tests were also examined. The noise label in a density-based method is not evidence that a cluster is irrelevant.

The silhouette coefficient s_i compares the mean distance a_i within the assigned cluster with the minimum mean distance b_i to another cluster, as given by Eq. (11).

$$s_i = \frac{b_i - a_i}{\max(a_i, b_i)} \tag{11}$$

For the mechanical datasets, five 80% resamples were evaluated using seed 2026. Assignment agreement was measured by the adjusted Rand index (ARI). Both ARI and silhouette assess internal clustering behavior. Neither is a measure of engineering priority, and cluster membership does not enter the ranking score.

5.3. Geometry, Network and Utilization Scores

Depth, edge-neighborhood count, and member utilization have different units and distributions. Each numerical feature x was transformed within its own scenario to an ascending fractional rank. Tied observations receive the mean rank. Equation (12) defines the transformation for a sample of size n.

$$p(x_i) = \frac{\mathrm{rank}_{avg}(x_i)}{n} \tag{12}$$

Let g = p(d), n_e = p(N), and m = p(U). The indicator r denotes a structural frame or column category. It equals one throughout the mechanical subsets but distinguishes categories in the full structural population. Equations (13) and (14) define the geometry-only (G), geometry–network (GN), and category-informed (R) scores.

$$S_G = g, \quad S_{GN} = \frac{g + n_e}{2} \tag{13}$$

$$S_R = 0.40g + 0.40n_e + 0.20r \tag{14}$$

When r is constant, R is a positive affine transformation of GN and the rankings are identical. Equation (15) defines the design-ratio-informed score M.

$$S_M = 0.35g + 0.25n_e + 0.10r + 0.30m \quad (15)$$

The weights sum to one and were not calibrated against expert ratings. Percentile transformation removes absolute magnitude; the original ratio U is therefore preserved for the review flag. Scores are rounded to 12 decimals and pair identifiers determine queue order. Displayed ties share the minimum rank.

For controlled ablation, $M_0 = (0.35g + 0.25n_e + 0.10r)/0.70$. Percentile ranks, ties, and the eligible population are held fixed. For a member queue, group eligible pairs by analytical member, take the maximum pair score, and break ties by ascending member identifier. Mean and median pair scores are evaluated as alternatives at the same member budget.

Equation (16) defines the fixed review budget K. The selected 10% is a comparison convention rather than an established risk threshold.

$$K = \lceil 0.10n \rceil \quad (16)$$

For the sensitivity analysis, each weight was changed by ±0.10, and the remaining weights were rescaled proportionally. Review budgets were rounded up to 5%, 10%, and 20% of the relevant pair or member population.

The resulting queue sizes are 33, 38, and 53 for A, B, and C, and 484 for full structural screening. Holding the queue size and underlying population constant isolates changes in selection from changes in review capacity.

5.4. Non-Compensatory Review Constraint

In Eq. (15), a low geometric or network score can offset a high mechanical percentile. Equation (17) introduces the binary flag F(c) using the original, unscaled design ratio. The primary ranking uses the frozen design bank at its exported precision. The targeted station reconstruction is reported separately.

$$F(c) = \begin{cases} 1 & U(c) \geq 1 \\ 0 & U(c) < 1 \end{cases} \quad (17)$$

For each mapped pair, compare the original design-bank ratio to the threshold before percentile transformation. Equality triggers review. Sort flagged pairs first by decreasing U, then by decreasing M rounded to 12 decimals, then by increasing pair ID. Sort ordinary pairs by decreasing rounded M and increasing ID. Missing U leaves the flag undefined. Retain flagged pairs beyond the review budget in an overflow register.

5.5. Comparison Measures and Sensitivity

Evaluation uses median U, distinct member count, Spearman rank correlation, and Jaccard overlap of the top-K sets. Equation (18) defines the latter. Because U is a scoring input, median enrichment is a measure of selection behavior rather than independent accuracy.

$$J(Q_1, Q_2) = \frac{|Q_1 \cap Q_2|}{|Q_1 \cup Q_2|} \tag{18}$$

Rank correlation describes the full ordering, whereas Jaccard overlap measures changes in the review queue. Counting distinct members reveals whether multiple pairs concentrate the queue around a smaller number of structural elements.

The mechanical weight w was varied from zero to 0.60 in increments of 0.10, while preserving the relative proportions of the other weights. Equation (19) defines the perturbed score.

$$S(w) = \frac{1-w}{0.70}(0.35g + 0.25n_e + 0.10r) + wm \tag{19}$$

The reference weight is 0.30. Setting w to zero does not exactly recover GN because the remaining weights differ. Feature ablation and six axis-translation perturbations of ±0.05 m examine local sensitivity.

6. Results and Discussion

6.1. Statistical Characteristics of the Clash Dataset

Aggregation accounts for 3,365 registrations beyond the unique-pair count, or 29.42% of the raw occurrences. Room-volume screening excludes another 777 pairs (9.62% of unique pairs). These reductions describe the data pipeline, not a reduction in site rework.

Structure–architecture pairs account for 62.29% of the filtered population (Table 3). The predominance is consistent with the extent of architectural boundaries and floor and wall surfaces. Of the 4,832 structural pairs, 1,568 involve frame members, and 642 involve columns. The remaining 2,622 involve other categories. Only 45.74% therefore fall within the frame or column classes; plate, connection, wall, and foundation resistance cannot be inferred from a frame utilization ratio.

Table 5 shows that the distributions of penetration depth vary across disciplines. Structure–MEP has the largest median, whereas structure–architecture has the largest 95th percentile. A

single penetration threshold would therefore select different proportions of each discipline group.

Table 5. Recorded penetration depths of filtered pairs (mm)

Pair type	Count	Mean	Median	95th pct.	Max.	Zero
Structure–MEP	287	47.14	49	109.40	131	21
Architecture–MEP	2464	28.36	19	82.70	392	17
Structure–architecture	4545	43.15	8	184.20	452	1368

The median depth for structure–MEP is 49 mm, about six times the 8 mm for structure–architecture. Yet the 95th percentile rises from 109.40 to 184.20 mm in the latter group. Of 1,406 zero-depth pairs, 1,368 belong to structure–architecture. Boundary contact, rounding, or model representation may explain these values, but none can be diagnosed by depth alone. Section 6.6 examines why excluding all zero-depth pairs can suppress a case that merits structural review.

6.2. Network Topology and Structural Screening

The graph has 3,139 vertices, 7,296 edges, and 11 connected components. The largest component contains 3,105 vertices (98.92%). The mean degree is 4.65, compared with a maximum of 163. This disparity indicates that a small part of the model is involved in many encounters. In the line graph, 189,487 adjacencies identify pairs sharing an element.

Both structural and architectural objects appear among the eight highest-degree vertices. Element 623964 has degree 163 and approximate betweenness 0.10969. Element 625409 has a lower degree of 140 but higher betweenness of 0.11559. Thus, the element with the most direct encounters need not occupy the most central position on network paths. Figure 6 shows the neighborhood of the maximum-degree vertex. Its layout represents topology rather than physical coordinates.

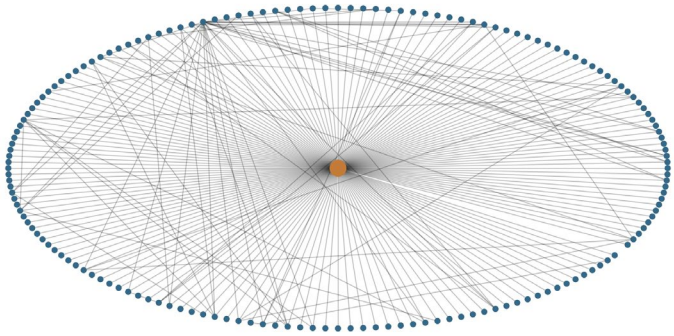

Figure 6. Neighborhood of the highest-degree vertex. A vertex identifies an element by source model and element ID. Each undirected edge represents one unique element pair. Degree counts distinct neighbors. A connected component joins vertices by paths of such edges.

In the full structural population, G, GN, and R each select 484 pairs. Their frame/column counts are 378, 209, and 464, respectively. The median depths are 175, 105, and 130.5 mm; the corresponding neighborhood counts are 33, 134, and 90. GN favors repeated encounters, whereas R concentrates the queue on the designated member categories. The change illustrates the trade-off between geometry and coordination context; it does not independently establish better engineering decisions.

6.3. Mechanical Data Coverage and Mapping Sensitivity

Table 2 identifies 18 members with strength ratios at or above unity: 17 composite beams and one column. In contrast, 119 composite beams have an unsuccessful overall design status. The reported serviceability median and maximum are 0.868 and 2.723. The discrepancy illustrates why overall status and strength utilization must not be used interchangeably.

Figure 7 shows the gain in mapping coverage from 329 to 377 pairs through beam segmentation and to 522 after conditional column association. The maximum ratio in B is 0.930, while that of the full composite-beam inventory is 1.937. Thus, the mapped beam subset omits the largest recorded strength ratios. The mechanical comparison cannot be generalized to every member in the analytical model.

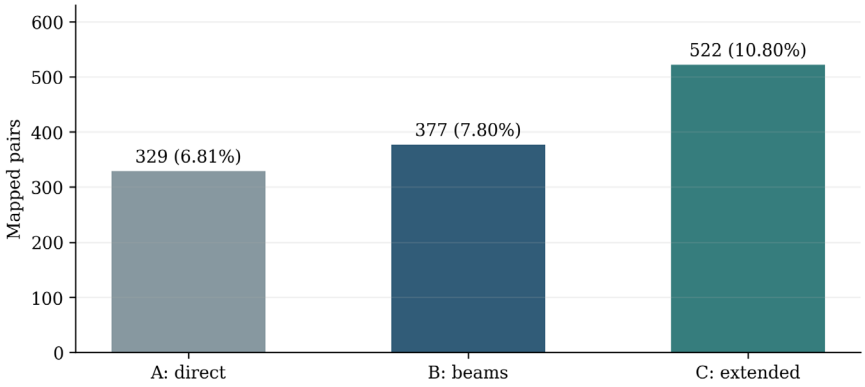

Figure 7. Mechanical mapping coverage relative to 4,832 structural pairs.

Of 114 initial section mismatches, only five were explained by recorded design-cycle changes. Another 506 pairs had geometry-only or elevation-only candidates and received no ratio. For plates and connections, 908 pairs had bounding information and a nearby candidate host, whereas 32 had no such host within the search radius. A host beam or column ratio cannot replace plate, bolt, or weld design checks. Excluding these matches prevents unsupported mechanical assignments.

The six translation tests (−X, +X, −Y, +Y, −Z, +Z) retained 522, 519, 518, 490, 501, and 522 pairs, respectively. Across all six tests, 475 pairs (91.0% of C) and 138 members retained their correspondence. The lowest coverage occurs for the +Y perturbation. This indicates direction-dependent sensitivity, but does not establish the accuracy of the rotation or model origins. Tightening the accepted-match cutoff from 150 to 75 mm retained 282 pairs on 88 beams. At 25 mm, 212 pairs on 71 beams remained. The corresponding overlaps with the original 38-pair queue were 29 and 20 pairs. These tests re-screened accepted identities and did not search for replacement members.

6.4. Unsupervised Characterization of Clash Patterns

Mixed-feature hierarchical clustering of the 4,832 structural pairs produced seven clusters with a silhouette of 0.7031. Their sizes (1,039, 536, 9, 685, 1,568, 353, and 642) coincide with the original member-category counts. Including category therefore largely recovers the original classes. Removing it yields three numerical clusters of 26, 1,797, and 3,009 pairs and a silhouette of 0.6110. The low agreement with the category grouping (ARI ≈ 0.104) shows that the numerical features describe a different partition.

HDBSCAN was sensitive to minimum cluster size. At 48, it returned 26 clusters and 743 noise observations; at 120, ten clusters and 347 noise observations remained. Non-noise silhouette increased from 0.6277 to 0.6733. Because the two values exclude different observations, they cannot establish that one solution is superior to the full-population hierarchical partition.

Table 6 summarizes the numerical clusters in the mapped populations. Each scenario contains two clusters. Cluster labels are arbitrary and must be interpreted through the feature profiles, rather than compared by their numeric labels.

Table 6. Numerical clustering and median feature profiles in mechanical subsets

Scenario/cluster	Pairs	Depth (mm)	Neighborhood	U median	Silhouette / ARI
A / 1	100	0.0	118	0.397	0.6725 / 1.0000
A / 2	229	73.0	11	0.437	—
B / 1	123	0.0	119	0.385	0.6495 / 0.9946
B / 2	254	74.5	11	0.415	—
C / 1	392	36.0	17	0.533	0.5409 / 0.9498
C / 2	130	0.0	119	0.385	—

In B, the two clusters have median depths of 0 and 74.5 mm and median neighborhood counts of 119 and 11. Their utilization medians, 0.385 and 0.415, are much closer. The distinction is therefore principally geometric and topological. In C, silhouette falls to 0.5409 and mean ARI to 0.9498. The change in composition may contribute to this decrease, but neither cluster can be interpreted as a structural risk class.

6.5. Comparison of Alternative Review Scores

Table 7 compares fixed-size queues within A, B, and C. R is omitted because its ranking equals GN in these subsets. All reported correlations and overlaps use M as the reference, so differences between scenarios do not constitute independent performance comparisons.

Table 7. Fixed-size review queues and agreement with mechanical ranking M (frozen design bank).

Scenario (K)	Score	Median U	Unique members	Spearman	Common pairs	Jaccard
A (33)	G	0.5330	23	0.643	17	0.347
	GN	0.4210	20	0.774	17	0.347
	M_0	0.4420	20	0.822	18	0.375
	M	0.8020	17	1.000	33	1.000
B (38)	G	0.6580	26	0.646	23	0.434
	GN	0.3850	24	0.768	16	0.267
	M_0	0.3850	23	0.808	18	0.310
	M	0.7885	19	1.000	38	1.000
C (53)	G	0.5330	33	0.496	28	0.359

GN	0.3870	31	0.730	27	0.342
M_0	0.3870	31	0.720	27	0.342
M	0.8020	25	1.000	53	1.000

In scenario B, the 38-pair queue under M had median utilization 0.7885 and covered 19 beams. Controlled ablation (M_0) gave a median of 0.3850 across 23 beams and retained 18 pairs in common with M. GN also gave 0.3850 but covered 24 beams and shared 16 pairs with M. Geometry alone (G) gave 0.6580 across 26 beams and shared 23 pairs with M. The choice of comparator therefore affects the estimated redistribution of review effort.

The same tendency appears in A and C. In A, the median changes from 0.421 to 0.802. In C, it changes from 0.387 to 0.802; 26 of the 53 selected pairs are replaced. Spearman correlations between GN and M are 0.774, 0.768, and 0.730 for A, B, and C, respectively. The corresponding Kendall coefficients are 0.5803, 0.5691, and 0.5384. Thus, the full ordering retains appreciable agreement even though the leading queue changes substantially.

Supplementary Figure S1 compares GN and M ranks in C. Points on the equality line retain their positions; deviations indicate promotion or demotion. A single uniform shift cannot explain the pattern because the geometric, network, and utilization percentiles vary between pairs.

Figure 8 shows that M selects higher-utilization pairs than G or GN in all three mapped populations. This is consistent with the direct inclusion of utilization in M. The results quantify a change in the composition of a fixed review budget, not predictive accuracy, failure probability, or time savings. Independent engineering ratings or intervention records would be needed to measure those outcomes.

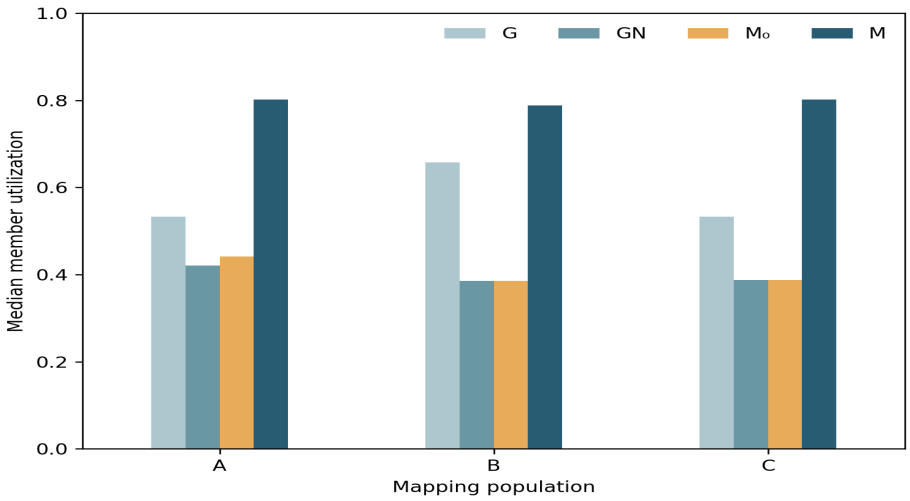

Figure 8. Median member utilization under G, GN, M_0 and M in each mapped population (frozen design bank).

The reduction in distinct analytical members is important for practical coordination. Several clash locations can be attached to one member-level review case, avoiding repeated structural assessments without discarding the individual geometric records.

6.6. Non-Compensatory Review and Column 627

Column 627 illustrates the principal limitation of a compensatory score. Its reported axial–flexural interaction ratio is 1.001, or 0.1% above unity. All nine conditionally associated pairs have zero penetration, placing them at ranks 185–253 under M. The high utilization percentile cannot offset the low geometry score. The result exposes a property of the ranking rule rather than a demonstrated design error.

Table 8 compares the 53-pair queues before and after mandatory review. Figure 9 depicts the observed rank intervals of the nine pairs; individual intermediate ranks are not inferred from the intervals.

Table 8. Effect of mandatory review in the conditional extended scenario (frozen design bank).

Metric	Compensatory M	Constrained M
Queue size	53	53
Pairs associated with U ≥ 1	0	9
Distinct corresponding members	0	1
Median U	0.802	0.871
Rank range of flagged pairs	185–253	1–9

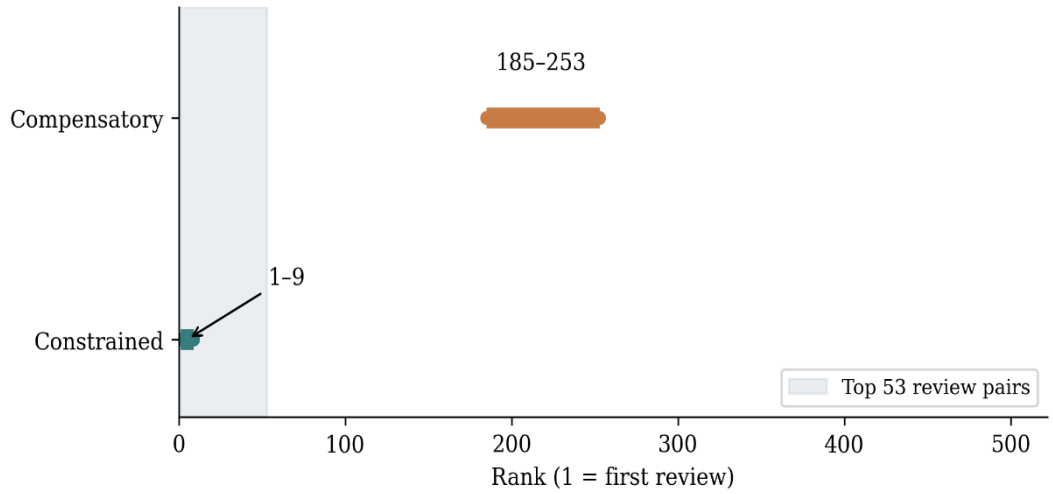

Figure 9. Reported rank intervals for the nine conditionally associated pairs of members 627.

The constrained 53-pair queue covered 21 members, compared with 25 under M alone. Nine positions referred to the same conditionally matched column. At a threshold of 1.00, all flagged ratios were identical, so ordering by utilization within flags preserved all 53 positions relative to ordering flags by score alone. At 0.90, 60 pairs representing 11 members were flagged. Seven entered the overflow register, and the two policies shared 47 of 53 selected pairs.

At station 0 m, ETABS 23.3.0 applies AISC 360-05 H1-1a under LRFD direct analysis with general second-order effects. The compression term exceeds 0.2. Adding eight ninths of each moment-to-capacity term reproduces both design summaries (Table 9). N2 governs the envelope even though both combinations display 1.001. The analytical length is 3.60 m with a 0.30 m J-end offset. Both seismic-ignore options are active; 1.02 is the software D/C limit. A ratio above the study referral threshold of 1.00 initiates review. This calculation verifies arithmetic using the capacities assigned in ETABS.

Table 9. Column 627 interaction check for assigned section 3IPE14FB1, Story2/C12. Values use the precision printed in the ETABS reports.

Station 0 m	G2	N2 (envelope)
|Pu| / ϕPnc (tonf)	109.6723 / 143.3035	109.6723 / 143.3035
|M33| / ϕMn33 (tonf·m)	2.2940 / 8.8417	2.2965 / 8.8417
|M22| / ϕMn22 (tonf·m)	0.0285 / 5.2221	0.0294 / 5.2221
Axial contribution	0.7653148737	0.7653148737
Major bending, weighted	0.2306243269	0.2308756612
Minor bending, weighted	0.0048511774	0.0050043724
Reconstructed H1-1a	1.0007903779	1.0011949073

The targeted export shares 119 steel members with the frozen design bank. At the exported precision, 35 member ratios differ by at most 0.007; member 627 is unchanged. Substituting only the targeted steel ratios in scenario C retains nine flagged pairs, changes their initial rank span from 185–253 to 182–253, and changes the constrained top-53 median from 0.871 to 0.867. The targeted workbook contains no replacement composite-beam summary. Primary results therefore retain the original design bank.

Partition eligible pairs into flags and ordinary cases. Sort flags by decreasing ratio, decreasing M, and ascending pair ID. Fill K positions with flags, then ordinary cases sorted by M and ID. Keep every remaining flag in a mandatory overflow register. At member level, deduplicate by analytical ID and retain all associated pair IDs.

6.7. Sensitivity to Scoring Weights and Feature Removal

Table 10 and Supplementary Figure S2 describe the response to mechanical-weight changes in C. Increasing w increases the median utilization of the selected pairs, while moving the weight

away from 0.30 reduces agreement with the reference queue. At w = 0.60, median U reaches 0.917, but Jaccard overlap falls to 0.452.

Table 10. Sensitivity to mechanical weight in scenario C (frozen design bank).

Mechanical weight	Jaccard vs. 0.30	Spearman	Median U
0.00	0.342	0.720	0.387
0.10	0.493	0.869	0.688
0.20	0.710	0.966	0.783
0.30	1.000	1.000	0.802
0.40	0.828	0.964	0.831
0.50	0.710	0.893	0.871
0.60	0.452	0.818	0.917

At w = 0.20 and 0.40, overlap remains 0.710 and 0.828, respectively, and Spearman exceeds 0.96. The ranking is therefore relatively stable close to the reference weight. Selecting w solely to maximize median U would favor a criterion already included in the score and could displace important coordination cases. Independent review evidence is needed for weight calibration.

In scenario B, M and M_0 shared 18 of 38 pairs (Jaccard index 0.310). Mean utilization increased from 0.5203 to 0.7218, and median utilization increased from 0.3850 to 0.7885. The number of unique beams fell from 23 to 19. At a separate budget of 12 of the 120 beams, aggregation by maximum, mean, and median pair score selected members associated with 78, 64, and 47 pairs, respectively.

Table 11 isolates the influence of each scoring component. Removing geometry gives Jaccard overlaps of 0.288 in B and 0.233 in C. Removing mechanics gives 0.310 and 0.342, respectively. Removing the network term changes fewer queue positions at the selected weights.

Table 11. Queue overlap and rank sensitivity to feature ablation (frozen design bank).

Removed term	A: J / ρ	B: J / ρ	C: J / ρ
Geometry	0.269 / 0.723	0.288 / 0.714	0.233 / 0.653
Network	0.610 / 0.874	0.689 / 0.866	0.683 / 0.842
Member class	1.000 / 1.000	1.000 / 1.000	1.000 / 1.000
Mechanics	0.375 / 0.822	0.310 / 0.808	0.342 / 0.720

In the full structural population, the mixed-feature cluster labels reproduced the member categories exactly (ARI and NMI both 1.000). Removing categorical features reduced agreement to ARI 0.104 and NMI 0.161.

The member-category term has no ranking effect in the mapped populations because it is constant. Geometry and mechanics make the largest contributions to changes in the leading queue. This is an internal sensitivity result, not a causal assessment of engineering outcomes.

6.8. Explainable Ranking and Decision Traceability

The additive score permits exact attribution of each ranking contribution. Let c_G, c_N, c_R, and c_M denote the four weighted terms of Eq. (15). Equation (20) expresses their sum for each pair.

$$S_M(c) = c_G + c_N + c_R + c_M \tag{20}$$

Table 12. Selected pair records and geometric versus combined rank in C (frozen design bank).

Pair ID	ETABS ID	Depth (mm)	Neighbors	U	G rank	M rank
3017	438	175	94	0.930	33	1
2993	442	175	73	0.907	33	2
3326	17	110	75	0.990	88	4
7264	627	0	42	1.001	405	185
7293	627	0	26	1.001	405	253

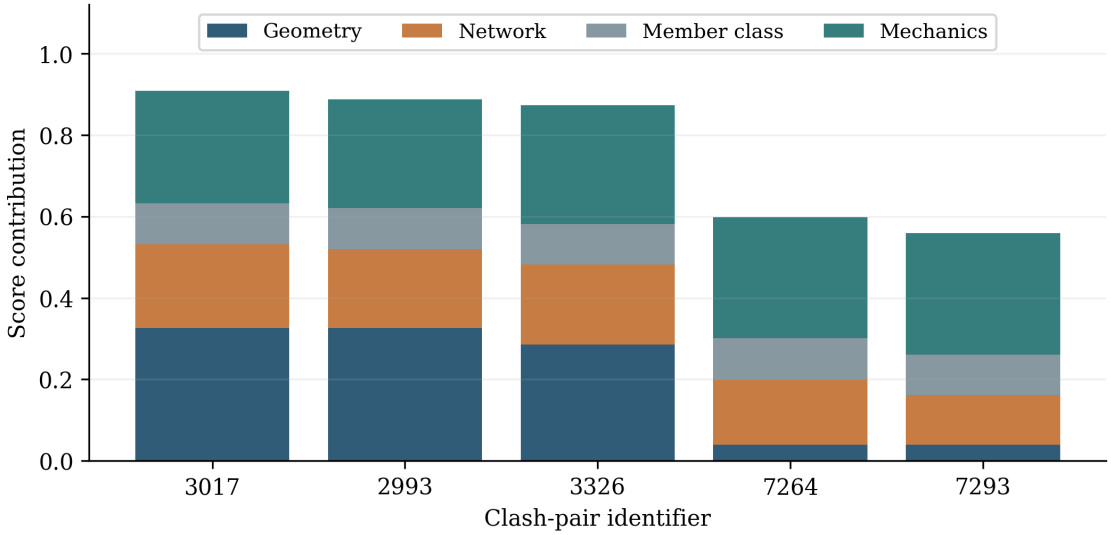

Figure 10. Exact contributions to the additive score in scenario C (frozen design bank). The category term is fixed at 0.10. The depth, neighborhood, and utilization terms vary with their within-population percentile ranks.

Table 12 and Figure 10 show how these contributions explain individual rank changes. Pairs 3017 and 2993 both have a penetration of 175 mm and a geometry contribution of 0.3265. Their network contributions differ (0.2052 and 0.1935), as do their mechanical contributions (0.2767 and 0.2675). The resulting scores are 0.9085 and 0.8875, subject to rounding. Pair

3326, with a conditional column match, has a mechanical contribution of 0.2917 compared with a geometric contribution of 0.2853. It moves from geometric rank 88 to combined rank 4.

Pairs 7264 and 7293 share a zero depth and a ratio of 1.001. Each has geometry and mechanical contributions of 0.0399 and 0.2977, respectively. Their network contributions differ (0.1607 and 0.1209), producing scores of 0.5983 and 0.5585. Both scores are too low for the initial top-53 queue. The mandatory flag changes their review order without modifying these contributions. The distinction makes the escalation decision directly traceable.

6.9. Position Relative to Published Approaches

Bitaraf et al. (2024) prioritize clashes using expert-derived weights and contextual criteria. The present study instead links the clash to a recorded member design ratio and separates mandatory review from compensatory scoring. Unlike the correction-sequence and change-prediction methods of Hu et al. (2020, 2023), it does not select a geometric modification. The published methods were not reproduced on identical data, and the planned blind expert assessment of 102 pairs has not yet been completed. Quantitative superiority and independent prioritization accuracy therefore remain unestablished.

7. Conclusions

Within the full composite-beam population, 119 records carried a Failed status. Seventeen met the strength threshold and the other 102 exceeded or equaled unity on a service check. All 17 strength-flagged beams had geometric candidates, but none had accepted B mappings.

This study examined the influence of structural design information on BIM clash review. The proposed method links physical elements to analytical members and combines their design ratios with geometric and graph features. A separate mandatory review rule addresses the limits of compensatory scoring. The main findings are as follows.

1. Aggregation and room-volume screening reduced 11,438 raw occurrences to 8,073 unique pairs and 7,296 filtered pairs. Of these, 4,832 involved structural elements. These are data-processing reductions rather than physical clash corrections.

2. The graph contained 3,139 vertices and 7,296 edges, with 98.92% of vertices in the largest component. Shared-element relations reveal coordination concentrations but do not establish load paths or correction dependencies.

3. Direct and segment-based beam mapping covered 377 pairs and 120 analytical members (7.80% of structural pairs). Conditional built-up column mapping increased coverage to 522 pairs and 148 members (10.80%). Unmapped utilization remained missing.

4. Numerical clustering of the structural population produced three clusters (silhouette 0.6110). In B, two clusters gave a silhouette of 0.6495 and a mean ARI of 0.9946. These groups describe feature patterns rather than independently verified risk classes.

5. In B, adding utilization to the controlled ablation increased the median from 0.3850 to 0.7885. Eighteen of the 38 pairs were common, and beam coverage fell from 23 to 19. Independent urgency ratings would be needed to determine whether these substitutions improve engineering decisions.

6. In C, nine zero-depth pairs conditionally linked to column 627 (interaction ratio 1.001) moved from ranks 185–253 to 1–9 after applying the non-compensatory rule. The top-53 median rose from 0.802 to 0.871. The nine pairs represent one column and require member-level verification before any correction.

7. Translation tests, weight sensitivity, and additive score decomposition provide internal evidence of traceability. Limited coverage, conditional column identity, and the absence of completed independent expert ratings prevent conclusions about safety improvement or superiority over published methods.

The proposed procedure provides a defensible record of why a clash is selected and why a particular member requires further review. Synchronized model versions and independent expert evaluation are needed before broader application.

Data Availability Statement

The study used project model exports from a shared building case. This analysis derives element-pair graphs, physical-to-analytical correspondences, and utilization-based review queues. Access to the project models, member identifiers, and pair-level data requires authorization from the data owner.

8. References

Abbasnejad, B., Ahankoob, A., Aranda-Mena, G., & Karamoozian, A. (2026). Artificial intelligence in BIM clash management: Assessment of current techniques, automation levels, and deployment readiness. *Buildings, 16*(13), 2623. https://doi.org/10.3390/buildings16132623

Ailem, R., & Boton, C. (2026). Automating clash relevance filtering in BIM-based multidisciplinary coordination using machine learning. *Automation in Construction, 181*, 106644. https://doi.org/10.1016/j.autcon.2025.106644

Akponeware, A. O., & Adamu, Z. A. (2017). Clash detection or clash avoidance? An investigation into coordination problems in 3D BIM. *Buildings, 7*(3), 75. https://doi.org/10.3390/buildings7030075

American Institute of Steel Construction. (2005). *Specification for structural steel buildings* (ANSI/AISC 360-05). https://www.aisc.org/ansi-aisc-360-05

American Institute of Steel Construction. (2010). *Specification for structural steel buildings* (ANSI/AISC 360-10). https://www.aisc.org/ansi-aisc-360-10

Bitaraf, I., & Shirzadi Javid, A. A. (2024). BWM-method prioritizing of clashes detected during the construction design phase with building information modeling (BIM). *AUT Journal of Civil Engineering, 8*(1), 51–66. https://doi.org/10.22060/ajce.2024.22593.5836

Bitaraf, I., Salimpour, A., Elmi, P., & Shirzadi Javid, A. A. (2024). Improved building information modeling based method for prioritizing clash detection in the building construction design phase. *Buildings, 14*(11), 3611. https://doi.org/10.3390/buildings14113611

Borkowski, A. S., & Kubrat, A. (2026). A conceptual AI-based framework for clash triage in building information modeling (BIM): Towards automated prioritization in complex construction projects. *Buildings, 16*(4), 690. https://doi.org/10.3390/buildings16040690

Bryde, D., Broquetas, M., & Volm, J. M. (2013). The project benefits of building information modelling (BIM). *International Journal of Project Management, 31*(7), 971–980. https://doi.org/10.1016/j.ijproman.2012.12.001

Campello, R. J. G. B., Moulavi, D., & Sander, J. (2013). Density-based clustering based on hierarchical density estimates. In *Advances in knowledge discovery and data mining* (pp. 160–172). Springer. https://doi.org/10.1007/978-3-642-37456-2_14

Freeman, L. C. (1979). Centrality in social networks: Conceptual clarification. *Social Networks, 1*(3), 215–239. https://doi.org/10.1016/0378-8733(78)90021-7

Gower, J. C. (1971). A general coefficient of similarity and some of its properties. *Biometrics, 27*(4), 857–871. https://doi.org/10.2307/2528823

Harode, A., Thabet, W., & Gao, X. (2024). Developing a machine-learning model to predict clash resolution options. *Journal of Computing in Civil Engineering, 38*(2), 04024005. https://doi.org/10.1061/JCCEE5.CPENG-5548

Hasannejad, A., Majrouhi Sardroud, J., Shirzadi Javid, A. A., Purrostam, T., & Ramesht, M. H. (2022). An improvement in clash detection process by prioritizing relevance clashes using fuzzy-AHP methods. *Building Services Engineering Research & Technology, 43*(4), 485–506. https://doi.org/10.1177/01436244221080023

Hu, Y., Castro-Lacouture, D., & Eastman, C. M. (2019). Holistic clash detection improvement using a component-dependent network in BIM projects. *Automation in Construction, 105*, 102832. https://doi.org/10.1016/j.autcon.2019.102832

Hu, Y., Castro-Lacouture, D., Eastman, C. M., & Navathe, S. B. (2020). Automatic clash correction sequence optimization using a clash dependency network. *Automation in Construction, 115*, 103205. https://doi.org/10.1016/j.autcon.2020.103205

Hu, Y., Castro-Lacouture, D., Eastman, C. M., & Navathe, S. B. (2021). Component change list prediction for BIM-based clash resolution from a graph perspective. *Journal of Construction Engineering and Management, 147*(8), 04021086. https://doi.org/10.1061/(ASCE)CO.1943-7862.0002092

Hu, Y., Xia, C., Chen, J., & Gao, X. (2023). Clash context representation and change component prediction based on graph convolutional network in MEP disciplines. *Advanced Engineering Informatics, 56*, 101896. https://doi.org/10.1016/j.aei.2023.101896

International Organization for Standardization. (2018). *ISO 19650-1:2018: Organization and digitization of information about buildings and civil engineering works, including building information modelling—Information management using building information modelling—Part 1: Concepts and principles*. https://www.iso.org/standard/68078.html

International Organization for Standardization. (2024). *ISO 16739-1:2024: Industry Foundation Classes (IFC) for data sharing in the construction and facility management industries—Part 1: Data schema*. https://www.iso.org/standard/84123.html

Koo, H. J., Guerra, B. C., Saka, S., & Leite, F. (2026). Streamlining BIM coordination and clash resolution through risk and relevance analysis. *Journal of Construction Engineering and Management, 152*(7), 04026092. https://doi.org/10.1061/JCEMD4.COENG-17676

Lin, W. Y., & Huang, Y.-H. (2019). Filtering of irrelevant clashes detected by BIM software using a hybrid method of rule-based reasoning and supervised machine learning. *Applied Sciences, 9*(24), 5324. https://doi.org/10.3390/app9245324

Liu, X., Zhao, J., Yu, Y., & Ji, Y. (2024). BIM-based multi-objective optimization of clash resolution: A NSGA-II approach. *Journal of Building Engineering, 89*, 109228. https://doi.org/10.1016/j.jobe.2024.109228

McInnes, L., Healy, J., & Astels, S. (2017). hdbscan: Hierarchical density-based clustering. *Journal of Open Source Software, 2*(11), 205. https://doi.org/10.21105/joss.00205

Mehrbod, S., Staub-French, S., Mahyar, N., & Tory, M. (2019). Beyond the clash: Investigating BIM-based building design coordination issue representation and resolution. *Journal of Information Technology in Construction, 24*, 33–57. https://www.itcon.org/2019/3

Newman, M. E. J. (2010). *Networks: An introduction*. Oxford University Press. https://doi.org/10.1093/acprof:oso/9780199206650.001.0001

Pärn, E. A., Edwards, D. J., & Sing, M. C. P. (2018). Origins and probabilities of MEP and structural design clashes within a federated BIM model. *Automation in Construction, 85*, 209–219. https://doi.org/10.1016/j.autcon.2017.09.010

Rezaei, J. (2015). Best-worst multi-criteria decision-making method. *Omega, 53*, 49–57. https://doi.org/10.1016/j.omega.2014.11.009

Rousseeuw, P. J. (1987). Silhouettes: A graphical aid to the interpretation and validation of cluster analysis. *Journal of Computational and Applied Mathematics, 20*, 53–65. https://doi.org/10.1016/0377-0427(87)90125-7

Rudin, C. (2019). Stop explaining black box machine learning models for high stakes decisions and use interpretable models instead. *Nature Machine Intelligence, 1*, 206–215. https://doi.org/10.1038/s42256-019-0048-x

Sacks, R., Eastman, C., Lee, G., & Teicholz, P. (2018). *BIM handbook: A guide to building information modeling for owners, designers, engineers, contractors, and facility managers* (3rd ed.). John Wiley & Sons. https://doi.org/10.1002/9781119287568

Succar, B. (2009). Building information modelling framework: A research and delivery foundation for industry stakeholders. *Automation in Construction, 18*(3), 357–375. https://doi.org/10.1016/j.autcon.2008.10.003

Teo, Y. H., Yap, J. H., An, H., Yu, S. C. M., Zhang, L., Chang, J., & Cheong, K. H. (2022). Enhancing the MEP coordination process with BIM technology and management strategies. *Sensors, 22*(13), 4936. https://doi.org/10.3390/s22134936

Yu, Y., Lee, H., Lee, W., & Koo, B. (2026). Transformer-based multi-view learning for BIM clash classification: Penetration taxonomy and constructability analysis. *Journal of Computational Design and Engineering, 13*(4), 227–251. https://doi.org/10.1093/jcde/qwag032